Remote Sensing and In-Situ Observations of Arctic Mixed-Phase and Cirrus Clouds Acquired During Mixed-Phase Arctic Cloud Experiment: Atmospheric Radiation Measurement Uninhabited Aerospace Vehicle Participation

G.M. McFarquhar, M. Freer, and J. Um
University of Illinois
Urbana, IL

R. McCoy and W. Bolton
Sandia National Laboratories
Livermore, CA

Introduction

The Atmospheric Radiation Monitor (ARM) uninhabited aerospace vehicle (UAV) program aims to develop measurement techniques and instruments suitable for a new class of high altitude, long endurance UAVs while supporting the climate community with valuable data sets. Using the Scaled Composites Proteus aircraft, ARM UAV participated in Mixed-Phase Arctic Cloud Experiment (M-PACE), obtaining unique data to help understand the interaction of clouds with solar and infrared radiation.

Many measurements obtained using the Proteus were coincident with in-situ observations made by the UND Citation. Data from M-PACE are needed to understand interactions between clouds, the atmosphere and ocean in the Arctic, critical interactions given large-scale models suggest enhanced warming compared to lower latitudes is occurring.

Flights

During M-PACE, the Proteus made 3 flights over mixed-phase clouds probing cloud structure with its lidar and measuring radiative fluxes with its suite of radiometers, and 2 flights over and through cirrus where both remote and in-situ observations were collected. The instruments are described in other posters presented by ARM UAV.

Table 1. Needs Caption

DATE	TARGET	LOCATION	DURATION	FLIGHT ALTITUDES	CLOUD ALTITUDE
Oct. 8, 2004	Multi-layer stratus	Barrow/Oliktok Point	5.5 hours	~ 13 km	Low
Oct. 9, 2004	Boundary layer stratus	Barrow/Oliktok Point	5.7 hours	~ 12.5 km	Low
Oct. 12, 2004	Boundary layer Stratus	Barrow/Oliktok Point	5.25 hours	~ 12. 5 km	~ 1 km
Oct. 17, 2004	Cirrus	Barrow	6.0 hours	7.5 to 12.5 km	5 to 10.5 km
Oct. 18, 2004	Cirrus	Oliktok Point	4.4 hours	7.5 to 13 km	4.5 to 8 km

Cirrus Observations – Remote Sensing

On October 18, 2004 the Proteus executed a series of racetrack profiles over Oliktok Point sampling cirrus between 8 and 4.5 km. Figure 1 shows the flight track together with cloud boundaries detected from the Cloud Detection Lidar. The cirrus was optically thin as the lidar penetrated cloud seeing the surface with few low-level clouds noted. After sampling the cirrus remotely, the Proteus descended into cloud measuring properties in-situ.

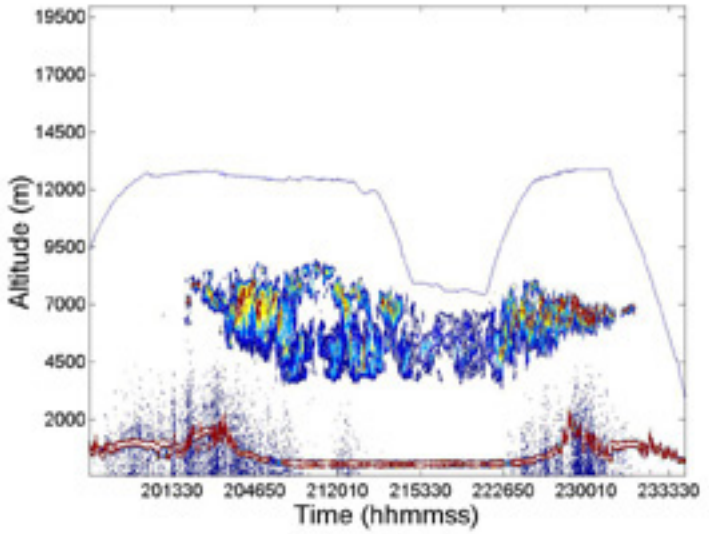

Figure 1. Uncalibrated lidar return as function of time for Oct. 18, 2004 flight above and through cirrus. Blue line designates the flight level of the Proteus.

Wang and Sassen's (2001) cloud detection algorithm was used to objectively determine the tops and bottoms of up to 10 cloud layers. For each layer, this algorithm provides top and bottom altitude, ratio of peak to base power, and tells whether the bottom is a true cloud base or virga layer base.

To provide users control over thresholds used to determine cloud boundaries, a graphical user interface (GUI) was developed in Matlab. This GUI (Figure 2) also allows users to control the time period over which data are plotted, whether tops and bottoms are overlaid on the lidar signal, and whether ASCII output files are generated. Output shown in Figures 3 and 4.

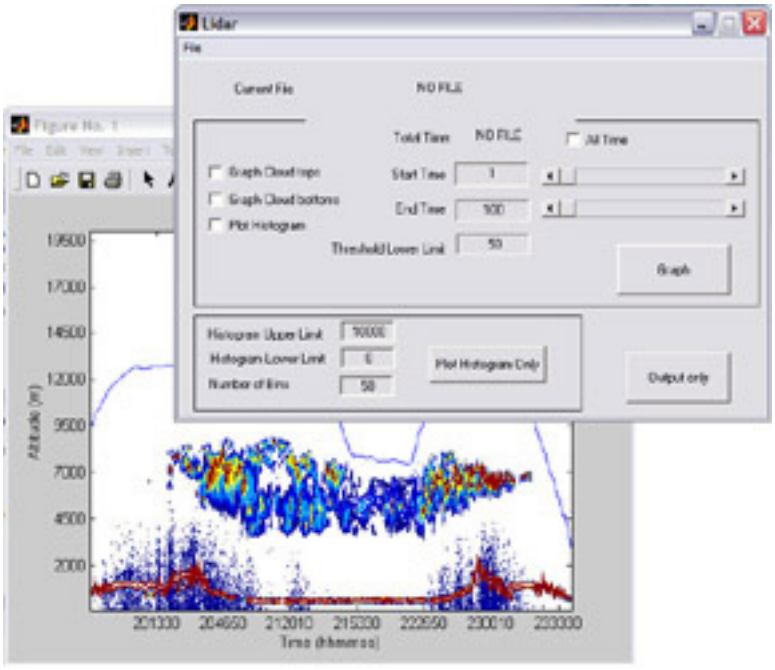

Figure 2. Example of GUI that runs in Matlab for identifying cloud boundaries.

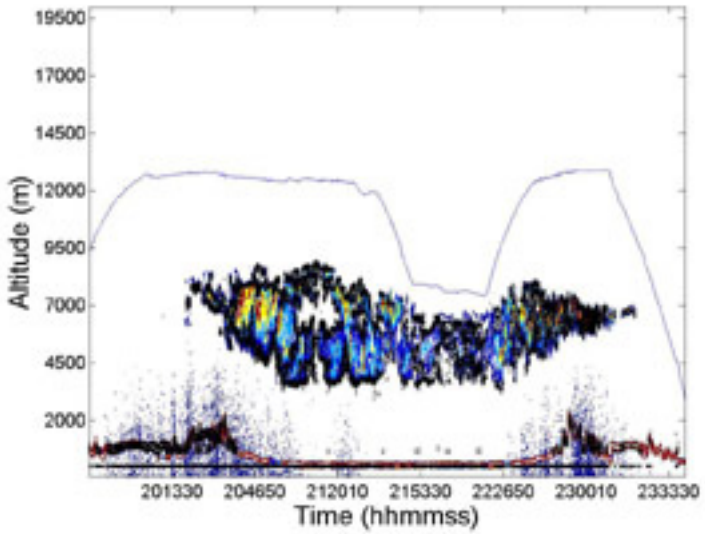

Figure 3. Cloud boundaries determined by applying Wang and Sassen detection algorithm to lidar signal displayed in Figure 1.

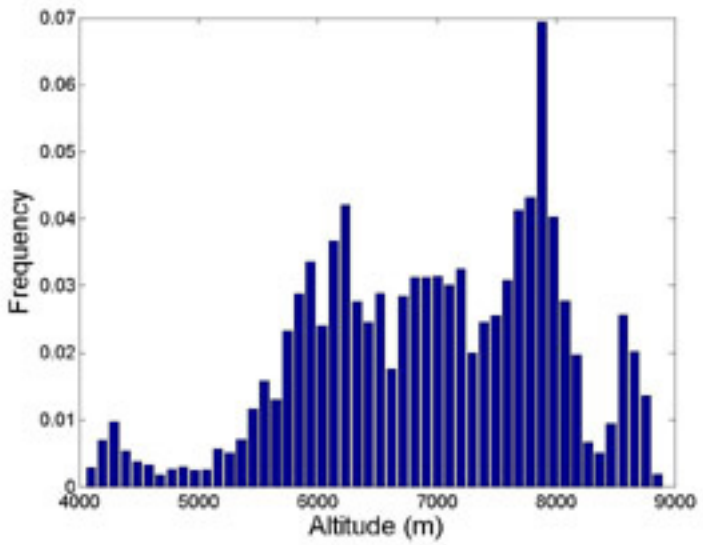

Figure 4. Histograms of normalized frequency of occurrence of cloud heights for October 18. Points with pitch angles > 5° excluded from analysis.

Cirrus Observations – In-situ Measurements

The Proteus has a cloud integrating nephelometer (CIN) that allows calculation of asymmetry parameter (g) and extinction coefficient (β_e) at l=0.635 mm light scattering observations obtained by 4 photo-multiplier modules. Using a running mean of 8 s to improve signal to noise, Figure 5 shows be as when the Proteus descended into cirrus.

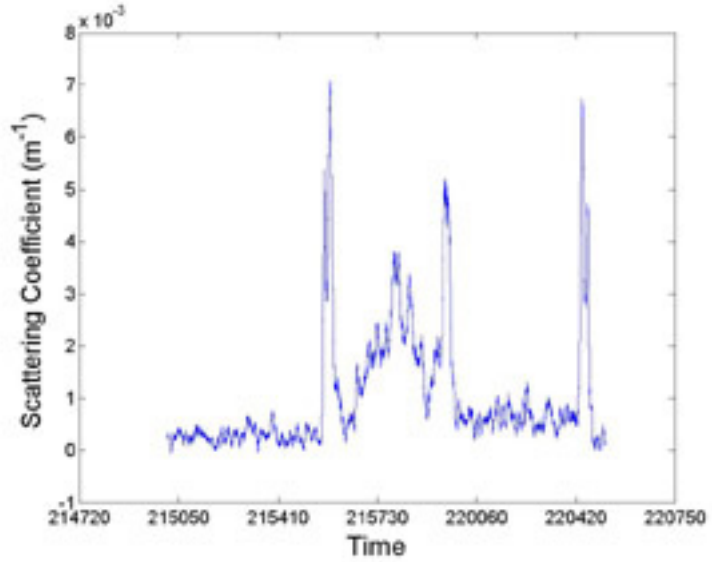

Figure 5. β_e from CIN as function of time for cirrus penetration; analysis suggested 8 s running mean optimum for data quality.

A GUI (Figure 6), developed to aid processing of CIN data, allows the user to control the plotting domain and averaging times for β_e and g.

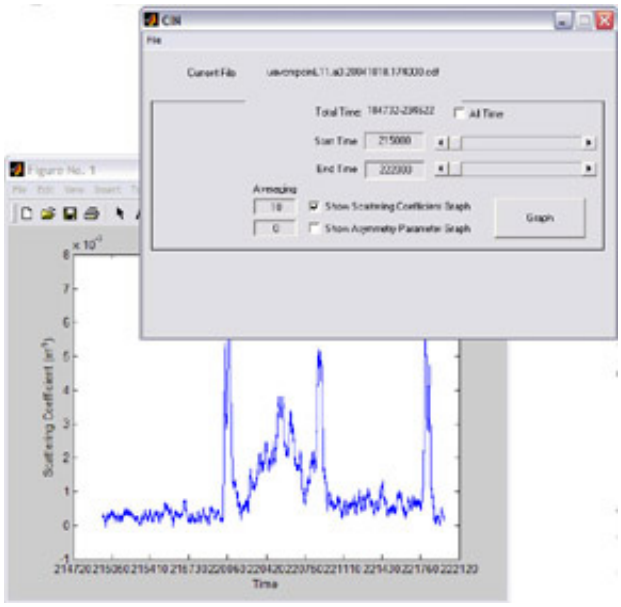

Figure 6. Example of GUI interface used in plotting CIN data.

Bulk cloud properties are also measured by the Nevzorov probe, a constant temperature hotwire probe with separate sensors for total water content (TWC) and liquid water content (LWC). Using a clear sky point just before descent into cloud and using a correction for altitude-dependent baseline drift allows estimates of TWC (Figure 7). Comparison with particle distributions from the CAPS should allow us to test consistency between CIN, Nevzorov and CAPS.

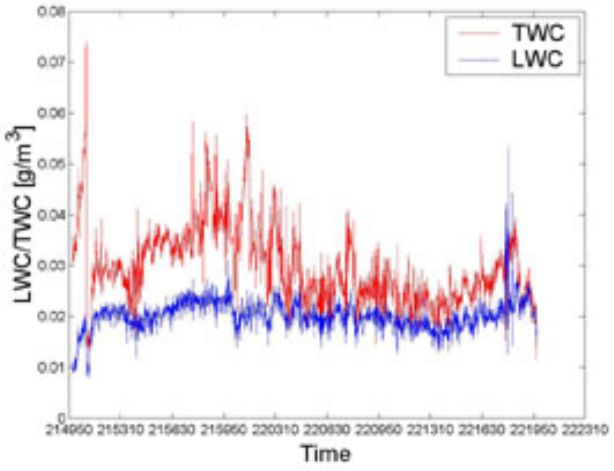

Figure 7. Nevzorov data from Oct. 18, 2004. LWC should be zero since measurements made in ice. Drift of baseline must be subtracted to estimate TWC.

Stratus Observations

On October 8, 9 and 12, 2004, the Proteus flew racetracks over Barrow and Oliktok Point, sampling boundary layer stratus with maximum heights of ~ 1 km. Figure 8 shows the profiles of uncorrected lidar return, showing the presence of low level stratus near the ground and few high clouds. Figure 9 shows the normalized frequency of occurrence of different cloud layers as determined by Wang and Sassen's (2001) detection algorithm.

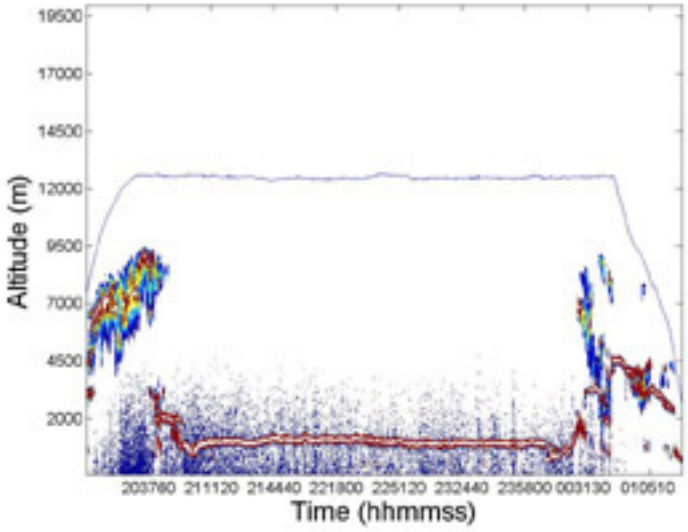

Figure 8. Uncalibrated lidar return as function of time for October 12, 2004 flight.

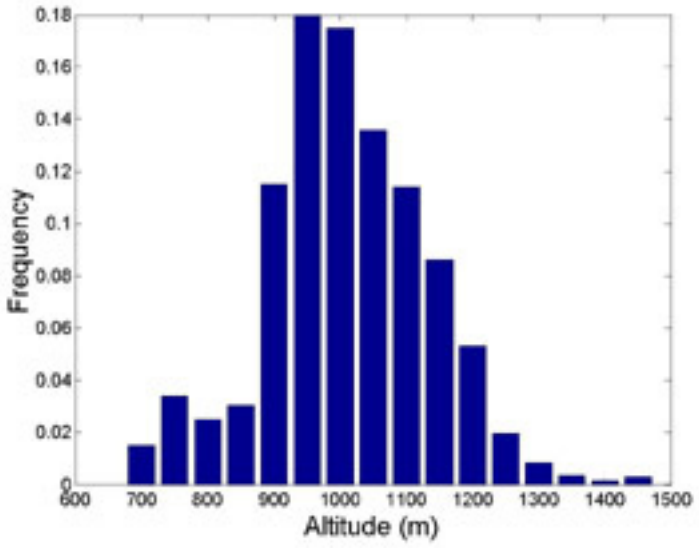

Figure 9. Histograms of normalized frequency of occurrence of cloud heights for October 12. Only leg between Barrow and Oliktok Point where pitch angle <5^{o} included.

In addition to the lidar, an infrared thermometer was available for retrieving cloud top temperature. Figure 10 shows the cloud top temperature measured by the infrared thermometer (IRT) on the October 8 flight over low-level stratus, and Figure 11 shows the spectrum of the IRT signal constructed in an attempt to determine if there are any characteristic frequencies in the IRT signal.

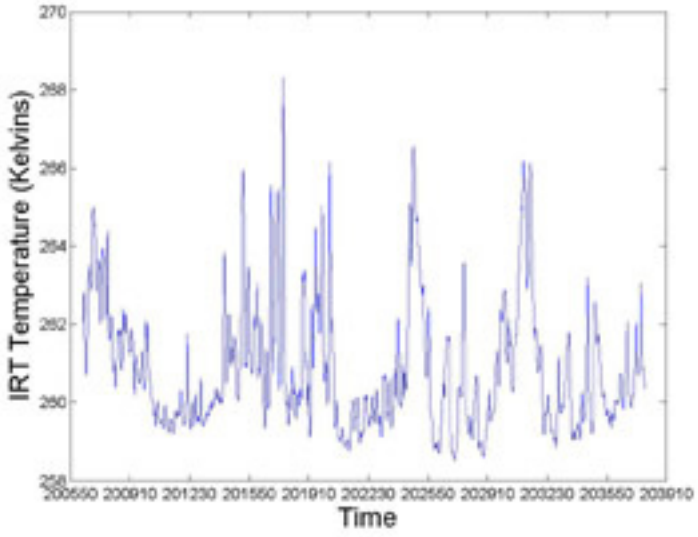

Figure 10. Cloud top temperature measured by IRT on October 8 above multi-layer stratus.

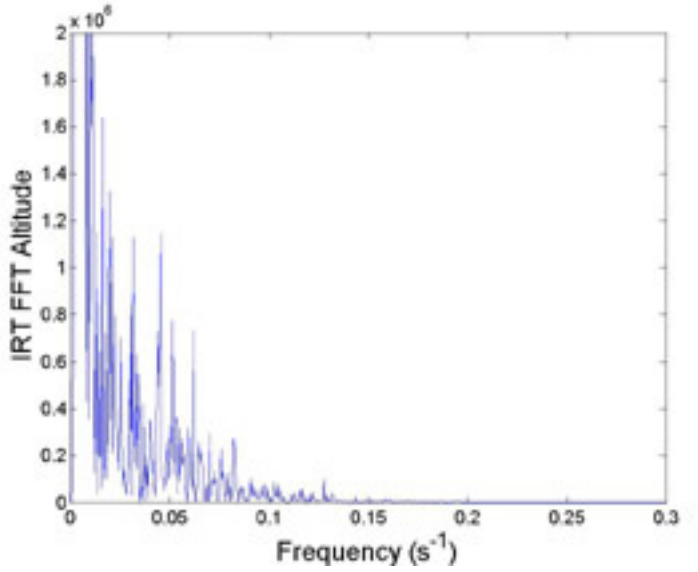

Figure 11. Spectrum of IRT signal in Figure 10 obtained using fast Fourier transform (FFT). Some preferred frequencies seen in signal.

Diffuse Field Camera Data

Remote measurements of scattering phase function by satellite (Baran et al. 2001) or aircraft flying in banked orbits (Francis et al. 1999) allows estimates of the dominant phase or particle habit. Using data from the 2002 ARM UAV flight series at the Southern Great Plains (SGP), we are exploring an alternate method for deriving scattering phase functions with the DFC.

The Diffuse Field Camera (DFC) consists of a pair of nadir-mounted digital camera with a HFOV lenses at 0.62-0.67 and 1.58-1.64 mm. They are most suitable for retrieving phase function when there is a horizontally uniform cloud layer with uniform surface characteristics below. Figure 12 shows examples of data obtained using the DFC for a flight over cirrus on November 23, 2002. These data can be used to retrieve information about the scattering phase function following the geometry outlined in Figure 13. Figure 14 shows the estimated phase function for this particular case. This is not an ideal case for calculating the phase function because the cirrus shown in Figure 12 is not horizontally uniform.

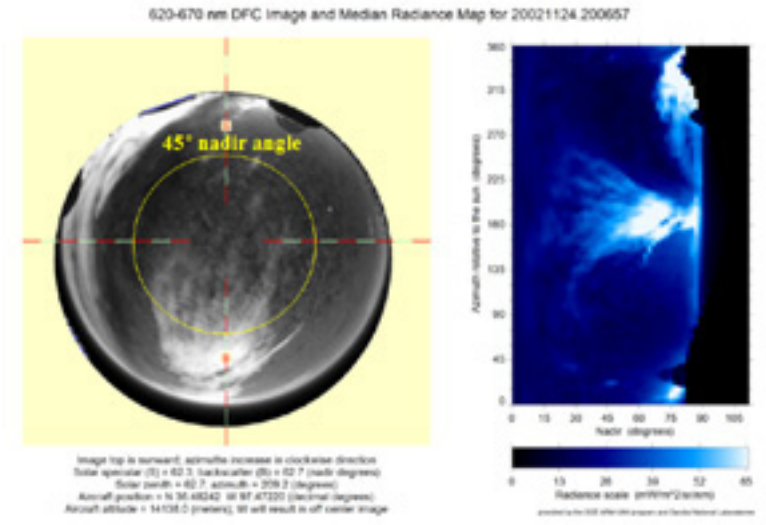

Figure 12. Example of DFC data from November 23, 2002. The figure on left shows image, whereas right-hand side gives radiance as function of azimuth relative to sun and angle from nadir.

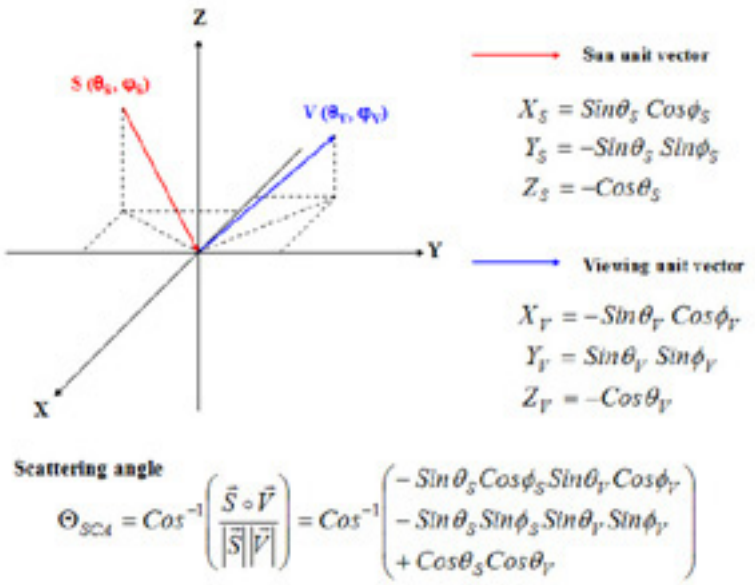

$$X_S = Sin\theta_S\, Cos\phi_S \qquad Y_S = -Sin\theta_S\, Sin\phi_S \qquad Z_S = -Cos\theta_S$$

$$X_V = -Sin\theta_V\, Cos\phi_V \qquad Y_V = Sin\theta_V\, Sin\phi_V \qquad Z_V = -Cos\theta_V$$

$$\Theta_{SCA} = Cos^{-1}\left(\frac{\vec{S}\circ\vec{V}}{|\vec{S}||\vec{V}|}\right) = Cos^{-1}\begin{pmatrix} -Sin\theta_S Cos\phi_S Sin\theta_V Cos\phi_V \\ -Sin\theta_S Sin\phi_S Sin\theta_V Sin\phi_V \\ +Cos\theta_S Cos\theta_V \end{pmatrix}$$

Figure 13. Schematic for calculating scattering angle from sun angle and viewing angle.

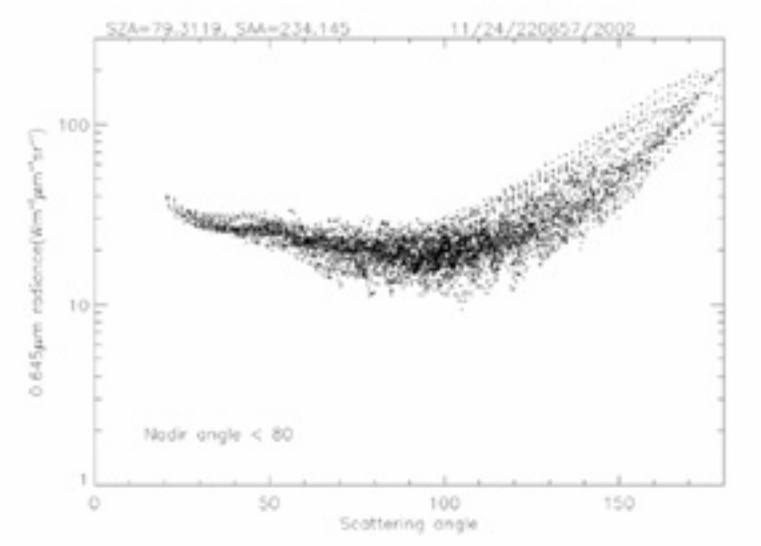

Figure 14. Example of phase function from Figure 11 image. Situation not ideal for retrieving phase function since surface reflectance seen through thin cirrus layer, which is not uniform.

Acknowledgments

This research was supported by the DOE ARM UAV program, Rick Petty program manager, and by DOE ARM under contract DE-FG03-00ER62913, Wanda Ferrell program manager. Data were obtained from the ARM archive sponsored by the U.S. Department of Energy, Office of Science, Office of Biological and Environmental Research, Environmental Sciences Division.

References

Baran, AJ, PN Francis, LC-Labonnote, M Doutriaux-Boucher. 2001. "A scattering phase function for ice cloud: Tests of applicability using aircraft and satellite multi-angle multi-wavelength radiance measurements of cirrus." *Quarterly Journal of the Royal Meteorological Society* 127:2395-2416.

Francis, PN, JS Foot, and AJ Baran. 1999. "Aircraft measurements of the solar and infrared radiative properties of cirrus and their dependence on ice crystal shape." *Journal of Geophysical Research* 104:31685-31695.

Wang, Z, and K Sassen. 2001. "Cloud type and macrophysical property retrieval using multiple remote sensors." *Journal of Applied Meteorology* 41:218-229.